

**ACOUSTIC EMISSION MONITORING ON STEEL-CONCRETE INTER-ACTION**

**SCHALLEMISSIONSMESSUNGEN ZUR UNTERSUCHUNG DES VERBUNDES ZWISCHEN STAHL UND BETON**

**MESURES D'EMMISSIONS ACOUSTIQUES POUR ETUDIER L'ADHERENCE ENTRE ACIER**

György L. Balázs, Christian U. Große, Rainer Koch and Hans W. Reinhardt

**SUMMARY**

Simultaneous registration of the acoustic emission (AE) signals and the bond-slip behaviour were carried out on pull-out specimens subjected to monotonic, cyclic and long term loads. The bond length was twice the rib spacing. Most of the signals were observed during an increase in load or applying the cyclic load, however, signals were registered during cycling and under constant load as well. The AE signal patterns were compared by applying the coherence spectrum analysis based on the fourier transforms of the signals. The internal damage accumulation, defined as the cumulative AE amplitudes, showed similar tendencies to the slip development both under cyclic and long term loads. The cumulative AE amplitudes include a point of inflexion in the region of bond strength for monotonic loading.

**ZUSAMMENFASSUNG**

Im Rahmen eines umfangreichen Versuchsprogramms wurden eine Reihe von Ausziehversuchen mit monotoner, zyklischer sowie Dauerstand-Belastung an Stahlbeton-Prüfkörpern durchgeführt; gleichzeitig wurden zerstörungsfrei die auftretenden Schallemissionssignale (SE-Signale) registriert. Die Verbundlänge wurde dabei entsprechend dem doppelten Rippungsabstand gewählt. Einerseits wurden die meisten SE-Ereignisse während der Lasterhöhung bzw. am Anfang

der Dauerschwingbelastung beobachtet, andererseits konnten auch eine Reihe von Signalen im Verlauf der statischen bzw. der zyklischen Belastung registriert werden. Auf der Grundlage der Fourier Transformation und einer anschließenden Berechnung der Kohärenz Spektren der verschiedenen Zeitsignale, lassen sich die Signalmuster im Hinblick auf die bruchmechanischen Vorgänge miteinander vergleichen. Eine statistische Auswertung der Schallemissionen zeigte darüberhinaus eine Abhängigkeit der Signal-Amplituden und damit der Schadensakkumulation vom gemessenen Schlupf, sowohl während der zyklischen als auch der Dauerstand-Belastung. Die kummulative Darstellung der SE-Amplituden zeigt einen Umkehrpunkt im Bereich der Verbundfestigkeit bei monotoner Last.

## RÉSUMÉ

Dans le cadre d'un programme de test volumineux on a effectué beaucoup d'épreuves de défournement avec une charge permanente, monotone et cyclique au spécimen du béton armé, simultanément on a enregistré les signaux d'émission acoustique (AE) non destructif. La longueur du composé était deux fois l'intervalle des nervures. La plupart des signaux étaient observés pendant qu'une augmentation de la charge et avec la charge cyclique tandis qu'il y en avait avec la charge statique et cyclique. Les figures d'AE signaux étaient comparées faire usage de l'analyse du spectre de cohérence basé sur la transformation de Fourier des signaux. L'accumulation de dommage interne (donnée la définition d'amplitude AE cummulative) montre des tendances semblable concernée le développement du glissement sous la charge cyclique et permanente. Les amplitudes AE cummulatives présentent un point de rebroussement dans la domaine de la contrainte d'adhérence pendant une charge monotone.

**Keywords:** interaction, local damage, damage accumulation, monotonic load, cyclic load, long term load, acoustic emissions, coherence spectrum

## 1. INTRODUCTION

Loads acting on the surface of a reinforced concrete element or the prestressing force applied on a pretensioned concrete element are transmitted by *interactional forces* from the concrete to the reinforcement or from the tendons to the concrete over the steel-concrete interface. The interactional forces produce relative displacement (slip) between the concrete and steel cross-sections indicating *local damages* in the concrete surrounding the reinforcing bars. Only low loads can be transmitted by physico-chemical adhesion.

*Micro-cracking* [1][2][3] and *micro-crushing* [4] are distinguished as local damages contributing to the increase in relative displacements or in crack widths. Cracks are considered to be micro-cracks until they do not reach the concrete surface. Crushing is localized to the loaded face of the bar lugs. The proportional contribution of micro-cracking and micro-crushing is still a matter of discussion. Test results indicating the existence of micro-cracks underline their importance, however, slip measurements by applying the Moirè-technique resulted in a higher contribution of micro-crushing to the actual slip.

Bond failure starts and progresses in the concrete layer surrounding the bar and leads to pull-out of the bar if the concrete cover is able to resist the circumferential tensile stresses to avoid splitting of the cover. *The acoustic emission (AE) technique* was chosen to detect the local damages in the concrete layer associated with acoustic effects at the energy release.

The experimental studies [5][6] indicated that the interactional behavior of a deformed reinforcing bar under monotonic loads is initially adhesional without slip, then mechanical interlock is provided which is followed by the

shearing-off by the concrete corbels between the bar lugs. This behavior can be demonstrated by the bond stress-slip relationship. The influence of the matrix strength [7], the deformation pattern of the reinforcing bar [8], the transverse stresses to the bar [9], the rate of loading [10], etc. are to be considered as well.

Cyclic [11][12][13] and long term [14][15] loads induce an increase in slip which may lead to pull-out failure indicating progressive local damages without an increase in the load. The damage accumulation under cyclic loads is tried to be predicted by linear [16][17] or by non-linear [18] rules for metals and for concrete, respectively.

The AE technique seems to be a very useful method for the investigation of local damages in the steel-concrete interactional layer because only signals of progressive local failures surrounding the reinforcing bar have to be recorded.

One of the advantages of the AE technique compared to other techniques to detect local damages within the interactional zone such as ink injection [1][2][3] or the application of Moirè-technique [4] is that it enables to register signals of the damage process during the entire load history without any disturbance on the specimen.

For many years the AE technique was used to detect the burst signals using one or even a few transducers to extract a set of parameters (like amplitude, trigger time, rise time, etc.) and to produce AE data for statistical analysis [19]. The classic recording equipment was not designed to record the events with a set of transducers and for storing the waveforms. Therefore a verification of the data was very difficult. The AE equipment has been

developed in the Otto-Graf-Institute [20] based on a transient recorder and a series of transducers for signal analysis in a comprehensive way.

*The purposes of this study were:*

- to analyse the time signals of the AE events in combination with the calculation of the coherence function as a mathematical tool for the comparison of AE signals,
- to analyse the amplitude and time distribution of AE signals in the steel to concrete interactional layer caused by various types of loads, such as monotonically increasing load, cyclic load and long term load, and
- to compare the load-deformation behavior to the accumulation of AE signals providing a basis for understanding of the progress of internal damages.

Due to the huge dataset, the amplitude and time distributions of the AE signals in addition to their waveforms are shown only for typical results. The evaluation of the recorded AE data with respect to a three dimensional localization is only partly presented herein and will be discussed in a separate paper.

## **2. TEST PROGRAMM**

The 14 pull-out tests were carried-out at the Otto-Graf-Institute in Stuttgart applying monotonically increasing deformations (6 specimens), cyclic loads (6 specimens) and long term loads (2 specimens).

## 2.1 Test specimen

The specimen was a concrete cube of 100 mm side lengths centrally reinforced with a single deformed bar of 16 mm diameter (Fig.1.b). A very short bond length, i.e. twice the rib spacing (20 mm) was used to minimize the number of sources producing local damages. The specimen had 80 mm unbonded length at the loaded side. The concrete cover was designed to provide the minimum cover eliminate splitting without applying transverse reinforcement.

The reinforcement had a nominal yield strength of 500 N/mm<sup>2</sup>. The measured average relative rib area was 0.065. The rib pattern consists of moonshape cross ribs and two longitudinal ribs (Fig.1.c).

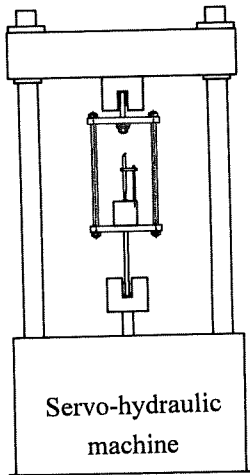
Mix proportions of concrete were 1 : 2.82 : 2.22 : 2.37 by weight of Portlandcement, fine aggregate (0 to 2 mm), medium size aggregate (2 to 8 mm) and coarse aggregate (8 to 16 mm). The water-cement ratio was 0.75. The specimens were vibrated for 15 seconds and fog-cured at a temperature of 20°C for 7 days and then were kept in laboratory conditions. The compressive strength at testing measured on cubes of 150 mm sides was 34,9 N/mm<sup>2</sup>.

## 2.2 Test setup

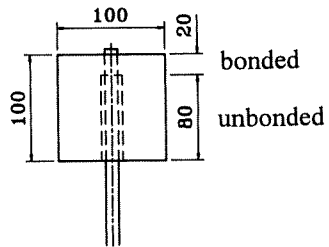
The specimens were tested in a servo-hydraulic machine (Fig.1.a) having a tensile capacity of 25 kN which is approximately 50 % higher than the pull-out strength of the specimens.

The tensile force acted on the reinforcing bar and the specimen was supported by a steel plate (Fig.1.a).

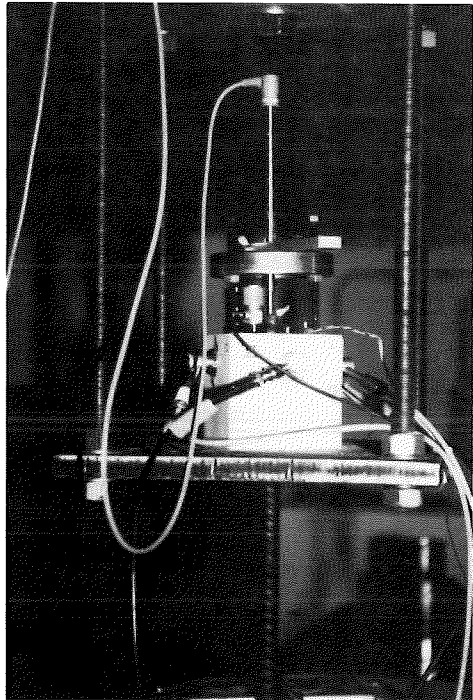
a) Test setup



b) Test specimen



d) Acoustic emission sensors and the LVDT



c) Rib pattern and section of reinforcing bar

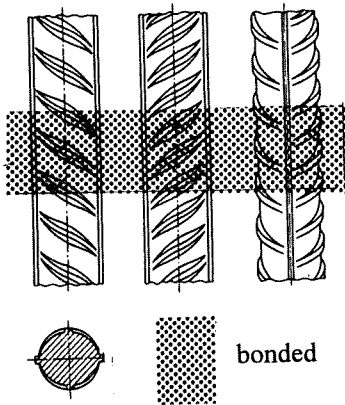


Fig.1 Test arrangement

## 2.3 Measuring system

The actual tensile force together with the relative displacements and the acoustic emission signals were registered simultaneously.

### 2.3.1 Slip measurements

The slip was measured by an LVDT of 1  $\mu\text{m}$  sensitivity at the unloaded end of the specimen.

### 2.3.2 Acoustic emission monitoring system

For the registration of AE signals a transient recorder with eight channels was used with a sampling rate of 1 MHz and an internal storing facility of 256 kWord for each channel (1 Word = 2 Byte). Using only the internal memory, 243 events could be recorded with a length of 1 kWord each. The amplitude resolution of each A/D-converter was 12 bit. The signals were recorded by eight piezo-transducers, coupled to the five sides of the specimens (Fig.1.d). Six had a so-called broadband characteristic (type UPE by GEOTRON and 8694 by KISTLER); two transducers operated in resonance (type 8612 by KISTLER) with a main frequency of about 20 kHz. They were amplified by an eight-channel preamplifier with a gain between 0 and 100 dB.

The amplifier was not supplied with gain ranging facilities so that the amplification has to be set manually and was adjusted during the experiments. This has to be taken into account when considering the presented amplitude values. On the other hand, it is important to realize that all amplitude

measurements have to be relative values due to the fact of locally different coupling conditions of the sensors even if they were adjusted in the same manner and with the same material (we used glue as couplant). For that reason all amplitudes are given in *relative peak amplitude* (PA) values and are only comparable in a single experiment.

An automatic gain ranging would match the gain of the amplifier to the amplitude of the incoming signal to achieve the best signal to noise ratio and to avoid the clipping of signals. This technique offers the best amplitude resolution and is normally used in seismology but not available for high frequency recording equipments.

We carefully paid attention to the electric decoupling of the AE monitoring system to prevent the recordings from the noise of the servo-hydraulic machine.

### **3. ACOUSTIC EMISSION SIGNALS**

Altogether 2500 complete AE events have been observed during the 14 pull-out tests. The signals (eight per event) that can be considered as *seismograms* were registered (on about 40 MByte) then plotted and catalogued. 80% of the events show a reasonable or a good signal to noise ratio and could be identified as AE signals.

The stress release in the specimen during the fracture process - investigated in this study - produces quasi its own signals. The basis for a detailed analysis is a localization of the events for being able to separate signals from noise and to assign the analysis results with local defects. The use of up

to eight transducers for signal recording meets the requirements for a three-dimensional localization analogy to the array technique in seismology - four sensors are the very minimum. To localize the events, the arrival times of eight seismograms have to be picked manually.

Selected results are presented in chapter 4 concerning the trigger-times and amplitudes of all AE signals and some of them are compared to each other.

### 3.1 Waveform analysis

The waveform of AE signals waveforms represent a lot of information about the fracture process. By recording the entire AE signal a comprehensive signal analysis can be carried out on the data.

Earlier it was difficult to interpret these informations because of the bad quality of data, the unproper equipments or the limits of available methods of analysis. Based on similar interests seismologists have shown several ways to evaluate informations on the source and the process of rupture together with its progress analysing the emitted waves. During the last years a couple of researchers [21, 22, 23] investigated the possibilities of an comprehensive signal analysis on the basis of the complete AE time signals.

One of the most important requirements is an extensive database of high quality, which means first of all broadband data with a good signal to noise ratio. The complexity of a time signal (as shown in the next few figures) does not always allow to draw quantitative conclusions. Very often *fourier spectra* of time series give a more accurate overview and allow a comparison of different events.

Comparing corresponding time signals, *the followings were observed.*

During one experiment *there are groups of signals with similar or almost the same waveforms*. Other signals show significant differences. These differences in waveforms among the signals of an experiment are sometimes greater than those in the various experiments.

To explain similarity and to show typical AE signals of pull-out tests, several events are plotted on the next few figures. **Fig.2.a** shows the seismograms of an acoustic emission event during a monotonic pull-out test (No.104, signed in the sequence of appearance; compared to the other traces, the seismograms of the resonant transducers (channel 5 and 6) are of restricted comparability because of their limited frequency range). According to the different locations of the sensors on the specimen, the onset time of the seismograms varies related to the different travel times. The source of AE signal originates from the close vicinity of the reinforcing bar while it produced concentric spreading of waves in all directions on very different paths through the inhomogenous concrete.

**Fig.2.b** represents another AE signal (No.27) from the same experiment, but from a different location. The waveforms of the signals show significant differences to those in Fig.2.a.

As stated above, we have found a couple of typical events with very similar or almost the same waveforms. The AE event No.120 shown in **Fig.2.c** was localized in the direct vicinity of No.104 and took place 72 seconds later (accompanied by 15 other events in between). An astonishing similarity between these two (and also ten other herein not presented) events can be realized even in the coda of the P-wave (that means the oscillations following the first puls of the compression wave) and in all details of the seismogram matches.

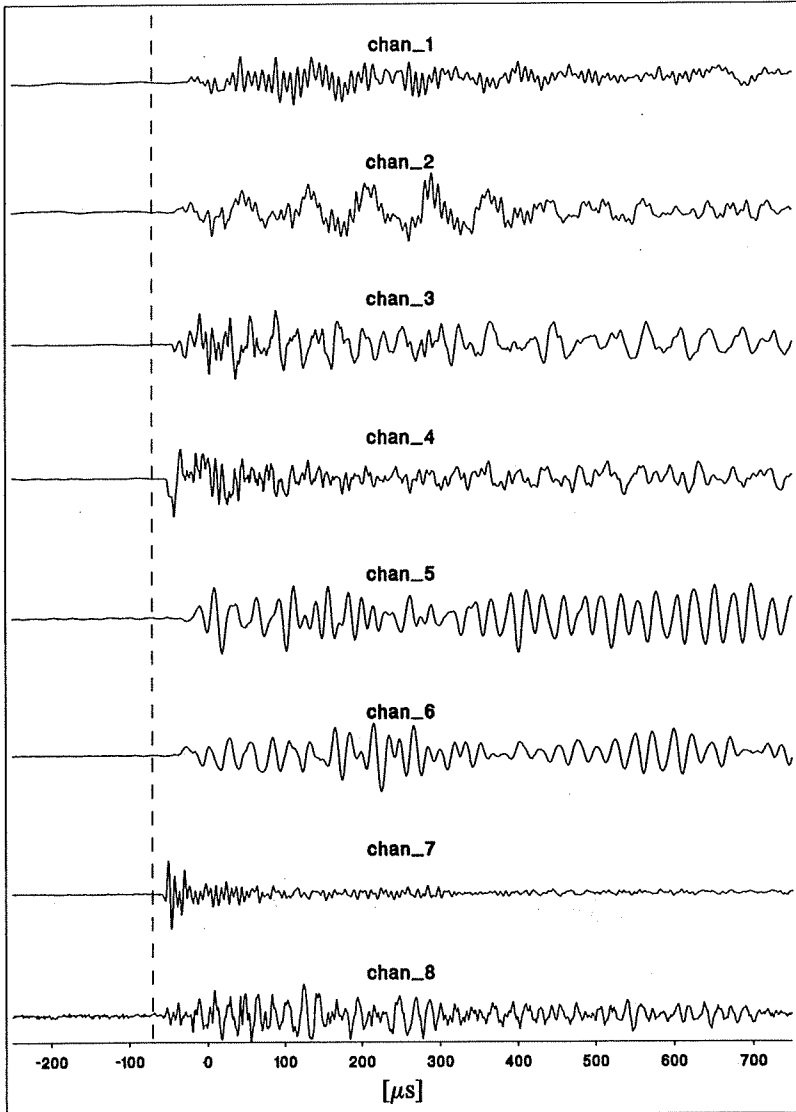


Fig.2.a Time signals of  
AE event no.104

5.12.1993



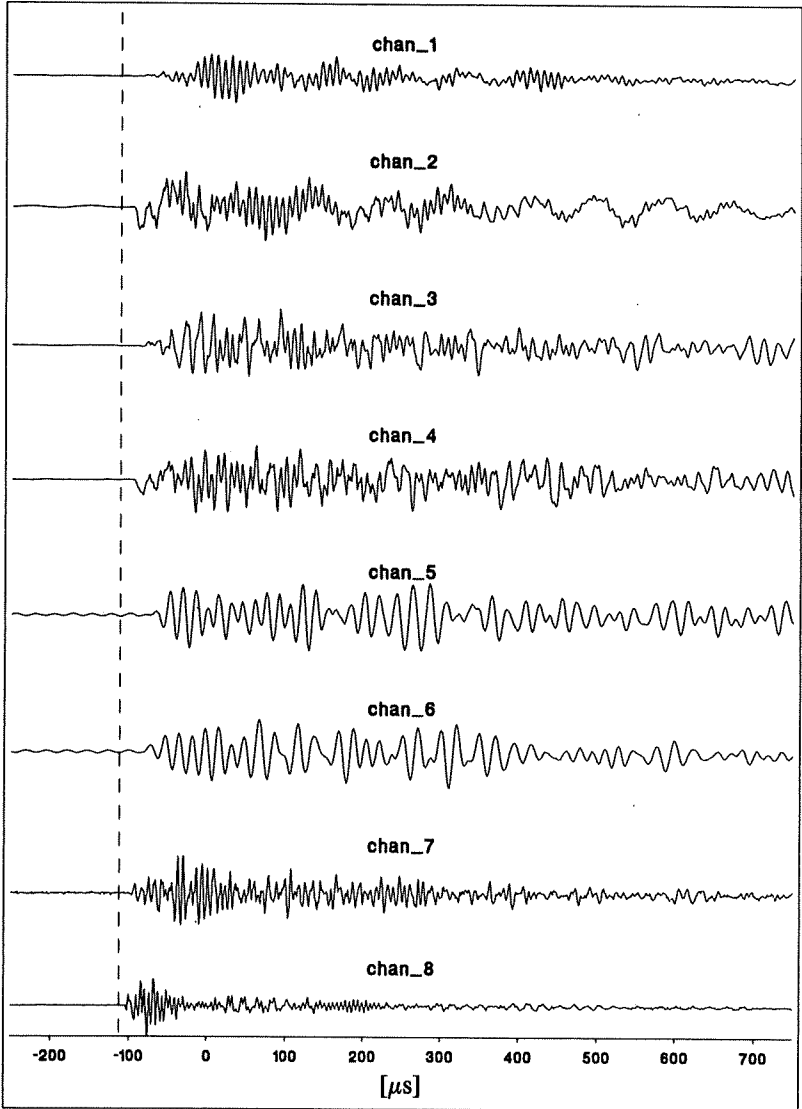


Fig.2.b Time signals of  
AE event no.27

5.12.1993



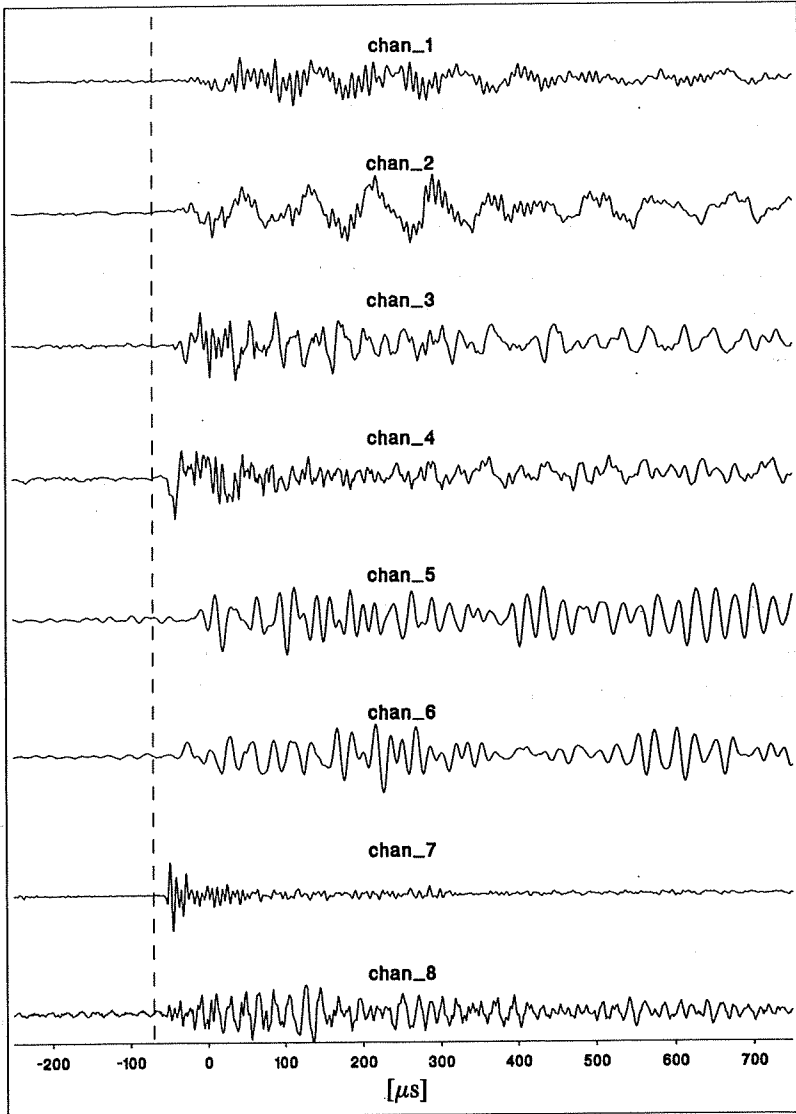


Fig.2.c Time signals of  
AE event no.120

5.12.1993

**EMPA**

### 3.2 Calculation of the signal-coherence

To quantify the above observations, we determined the coherence function of the signals.

The analysis of a seismogram commonly bases on the fourier spectrum of the time series. *The fast fourier transform* (FFT) is used to transform the time series to a frequency domain [24, 26]. The real components and the imaginary components of the FFT function is defined as

$$F(v) = \frac{1}{N} \sum_{t^*=0}^{N-1} X(t^*) \exp \left( \frac{-j 2\pi v t^*}{N} \right), \quad v = 0, 1, \dots, N-1 \quad (1)$$

In addition to, it is necessary to calculate the coherence of the power spectra (density power spectra, respectively) of the two signals and the cross spectrum. If the autospectrum of signal one is defined by

$$G_{xx}(k) = \sum_{n=1}^N |X_n(k)|^2 \quad (2)$$

and of signal two by

$$G_{yy}(k) = \sum_{n=1}^N |Y_n(k)|^2 \quad (3)$$

Then the cross spectrum is expressed by

$$G_{xy}(k) = \sum_{n=1}^N \hat{X}_n(k) Y_n(k) \quad (4)$$

The coherence spectrum results [25] from the squared cross spectrum divided by the product of the two autospectra

$$C_{xy}(k) = \frac{|G_{xy}(k)|^2}{G_{xx}(k) G_{yy}(k)} \quad (5)$$

Eq.5 provides a mathematical tool for comparing AE signals with respect to their similarity. Two absolutely identical signals would give a coherence with a value of one over the entire frequency range. Coherence values up to 0.5 indicate signals with different characteristics.

The coherence spectra of the signals shown in Figs.2.a to 2.c are presented in Figs.2.d and 2.e. It is reasonable to compare only the same channels (i.e. only the same subfigures) owing to the locally different coupling conditions and transfer functions of the sensors. To avoid spectral leaking, the FFTs are smoothed by a Hamming-window [26].

Fig.2.d shows the coherence functions for very similar signals (No.104 and No.120). The coherence is close to one over a wide frequency range. For frequencies beyond 300 kHz (channel 5 and 6; beyond 150 kHz) the influence of the high-frequency noise becomes dominant and the coherence is decreasing.

Fig.2.e presents the coherence functions for the other two signals No.104 (Fig.2.a) and No.27 (Fig.2.c). They are calculated for every single channel.

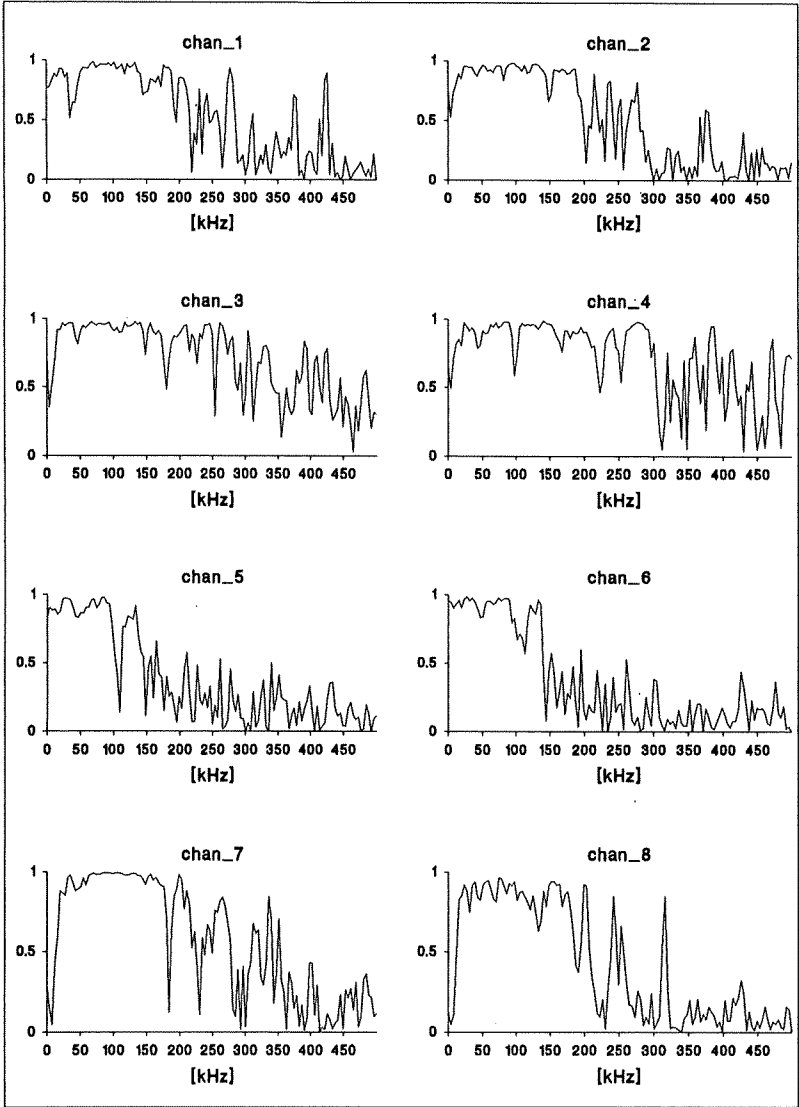


Fig.2.d Coherence functions of AE event no.104/120



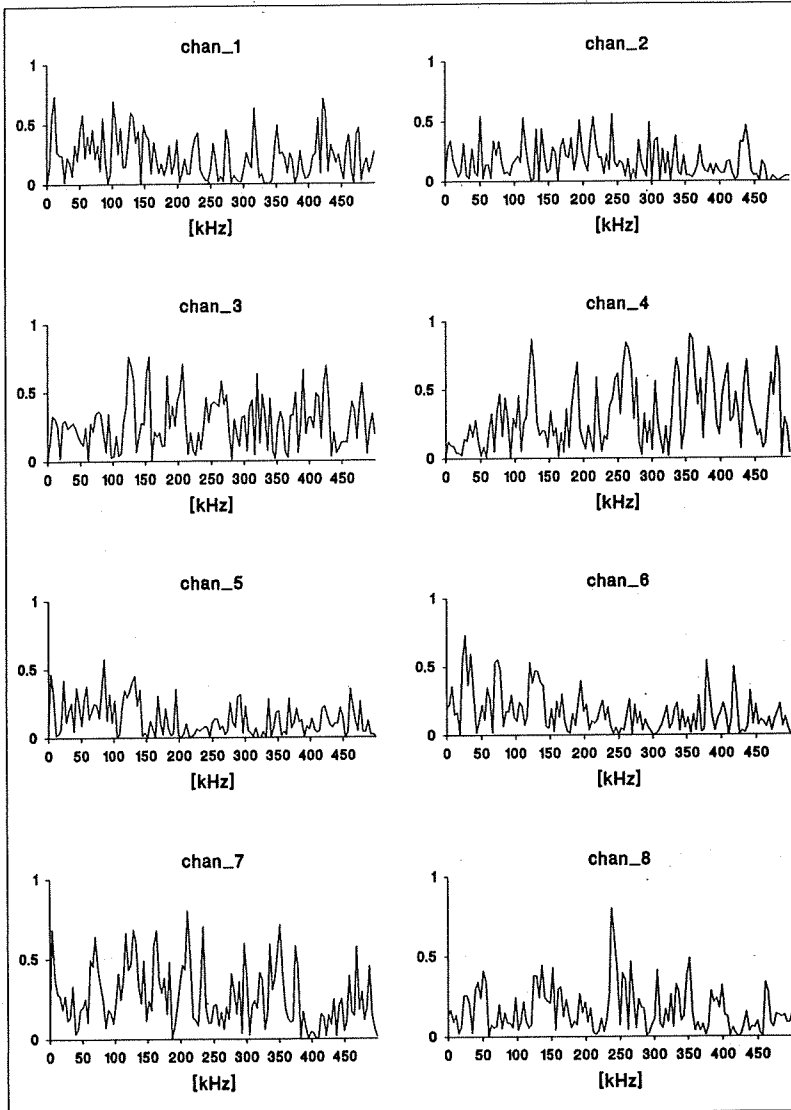


Fig.2.e Coherence functions of  
AE event no.104/27

**EMPA**

The coherence values of about 0.5 indicate that these signals are not very similar.

Assuming that the coherence functions for two signals show about the same course for different channels, it is possible to find a figure that represents the overall coherence. We calculated the mean coherence of the coherence functions for a pair of dataset and determined the *coherence sum*  $C_{xy}$  as the area below the curves using a numeric integration. The functions of the mean coherence (excluding channels 5 and 6) are given in Fig.2.f for the signals No.104 and No.27 (top figure) in addition to No.104 and No.120 (bottom figure) between 0 and 300 kHz (grey area). The coherence sum, meaning the area under the curves is 229 respectively 72. A perfect coherence in the frequency range of 0 to 300 kHz would result in a value of 300.

With a fourier analysis of the time series and the calculation of the coherence functions it is, therefore, possible to find a quantitative relationship between the waveforms of similar signals. This method is intended to be used for systematic classification of the AE signals with the automatic deduction of the coherence sum to recognize similarities and differences in signal patterns.

#### 4. DISCUSSION OF TEST RESULTS

Typical test results together with the comparisons for the bond-slip behaviour and the AE registrations are discussed separately for the three types of applied loads, i.e. monotonic, cyclic and long term loads, respectively.

The AE registrations are plotted in a statistical way using bars to give a survey over the appearances and amplitudes of the events related to the applied

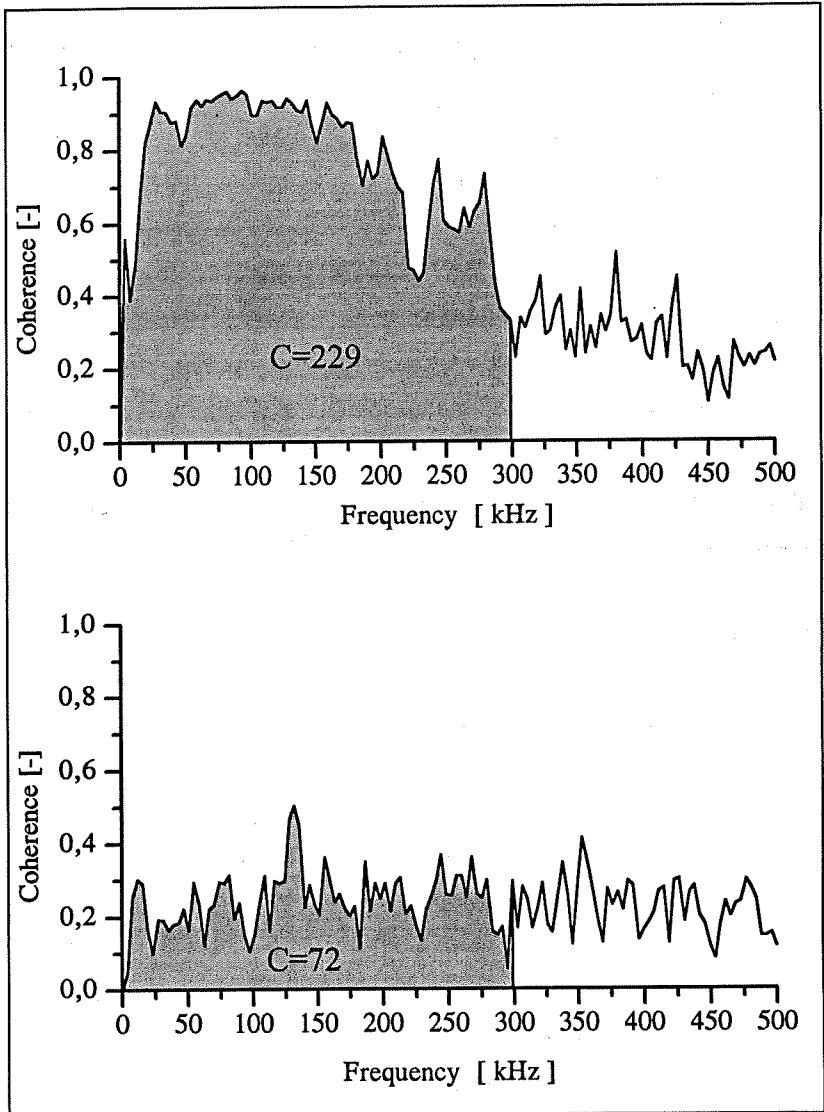


Fig. 2.f Mean coherence functions of signals 104/120 (top) and No. 104/27 (bottom).  
 The coherence sums are calculated for the range 0-300 kHz [dashed].

load. A direct presentation of the single amplitudes is unreasonable while the AE energy is often released abruptly, hence, a couple of events are registered in a very short time. Therefore, the time axis is divided into intervals of 10, 15, 25, 50 or 5500 seconds adjusting it to the duration of the given test.

In the upper part of the following figures *the amplitudes are given in relative values of the maximum peak-to-peak-values* of the signals (and denoted as PA sum per time unit). The AE bar graphics are generally presenting the statistics of a single channel (channel 1 with broadband transducer UPE), however, the statistics of all eight channels are shown in **Fig.3** for the pull-out test result with monotonic load discussed in **Fig.4** to confirm that the courses of the graphs are very similar. In the lower part of the following figures the amplitude values are plotted in a *cummulative* way to demonstrate the total amount of released energy (and are called cumulative PA).

#### **4.1 Monotonic Pull-out tests**

The continuous line of **Fig.4** shows the measured bond stress versus time relationship and the coloumns show the observed relative AE amplitudes summed in 10 second intervals. The two completely independent ways of measurement indicate *similar tendencies*. The highest AE amplitudes per interval were registered in the region of highest bond stresses then both were decreased.

The corresponding slip is shown in **Fig.4.b** having a non-linearly increasing tendency up to the bond strength followed by a linear one. (This diagram only indicates the non-linear bond behaviour at the beginning of loading and then reflects the deformation controlled loading having a constant

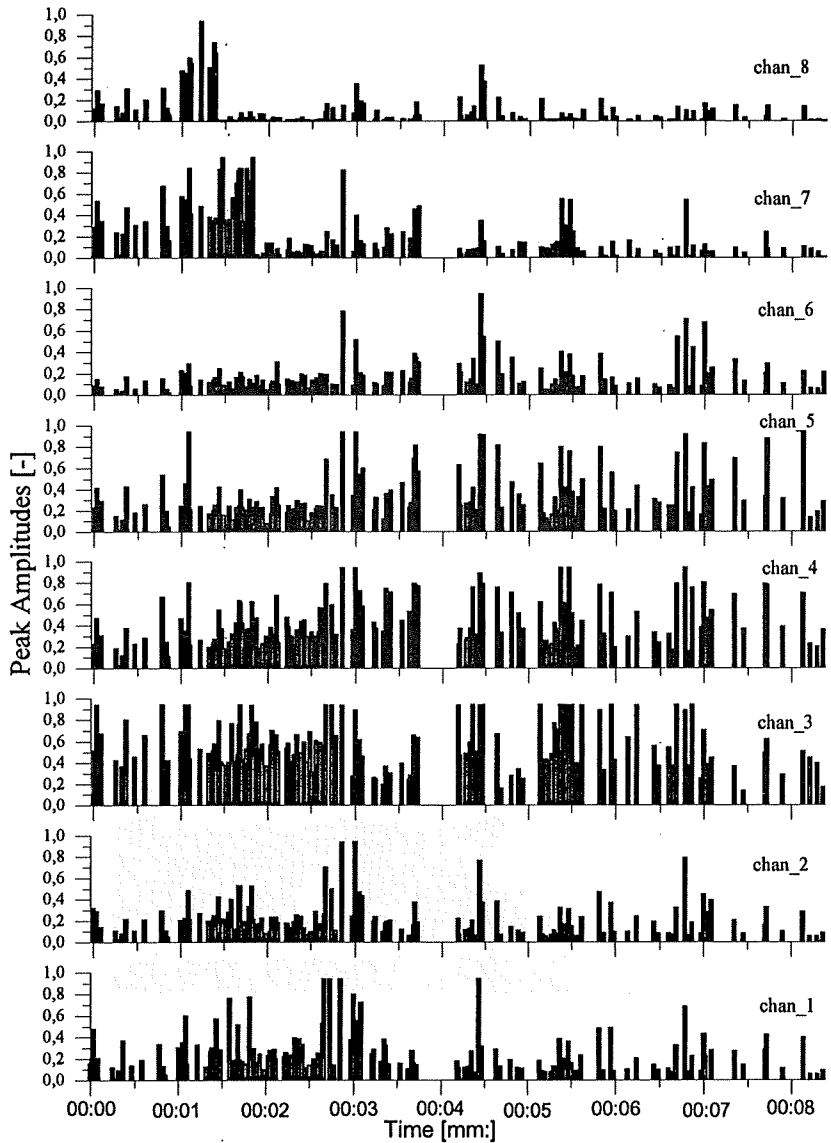


**Fig.3** Peak amplitudes (PA) for pull-out test with monotonic load.

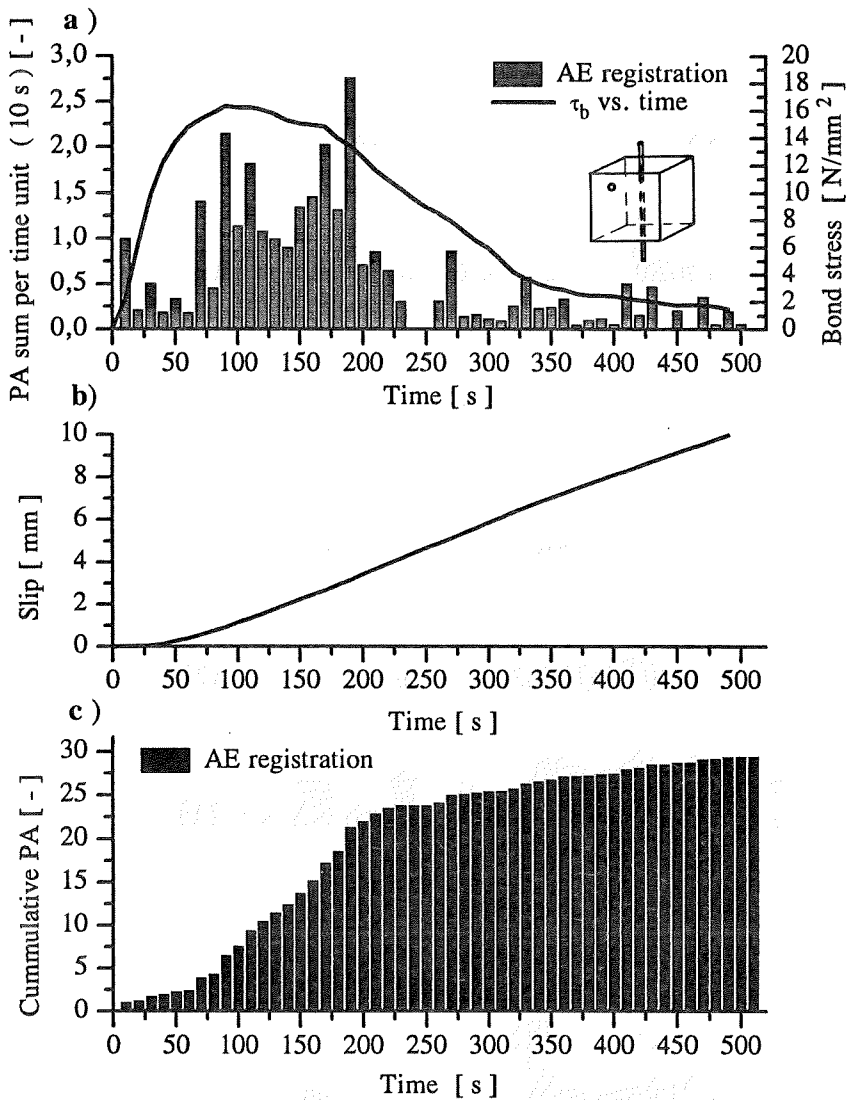


**Fig.4** Pull-out test detecting acoustic emission signals ( $\varnothing 16$ ,  $\alpha_{sb}=0.065$ ,  $f_y=500$  N/mm<sup>2</sup>,  $l_b=20$  mm,  $f_c=35$  N/mm<sup>2</sup>)

**a)** PA sums in 10 sec intervals and bond stress vs. time

**b)** Slip vs. time

**c)** Cumulative AE amplitudes vs. time

rate, however, it gives the slip values to the bond stresses at a given time. This representation was chosen because the bond stress-slip relationship would give a very similar diagram to the bond stress-time relationship.)

The accumulated damage is presented as the sum of all preceding acoustic emission amplitudes as a function of the time in **Fig.4.c**. The course of *accumulated AE amplitudes has a point of inflexion in the region of reaching the bond strength.*

The average bond stress based on five deformation controlled pull-out test results resulted in  $\tau_{bu} = 15.4 \text{ N/mm}^2$ . The loading rate was 0.02 mm/sec applied on the hydraulic machine.

## 4.2 Cyclic tests

**Figs.5, 6 and 7** indicate the pull-out test results under cyclic loading of 4 Hz frequency on one or more load levels.

The upper parts of these figures show the load history starting with an increasing load up to the mean value of the cyclic load together with the registered acoustic emission amplitudes summed in 10 or in 15 s intervals depending on the lengths of the test. Most of the AE signals are registered at applying the initial monotonic load up to the mean value of cyclic load, then at the beginning of the cyclic load, then at an increase in the cyclic load level and preceding the pull-out failure, however, some signals are detected during cycling with constant amplitudes as well.

The bottom parts of the same figures present the accumulated damage as the sum of the AE amplitudes as a function of the time together with the development of slip indicating a *similar tendencies*.

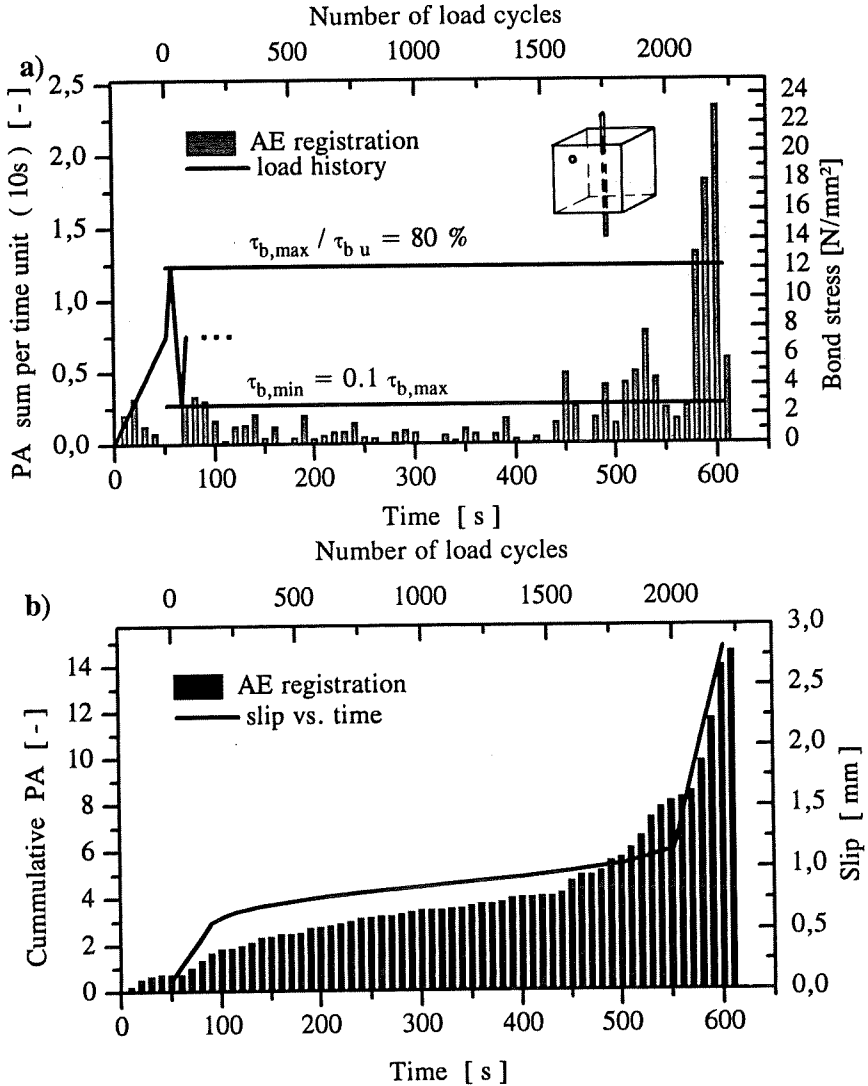
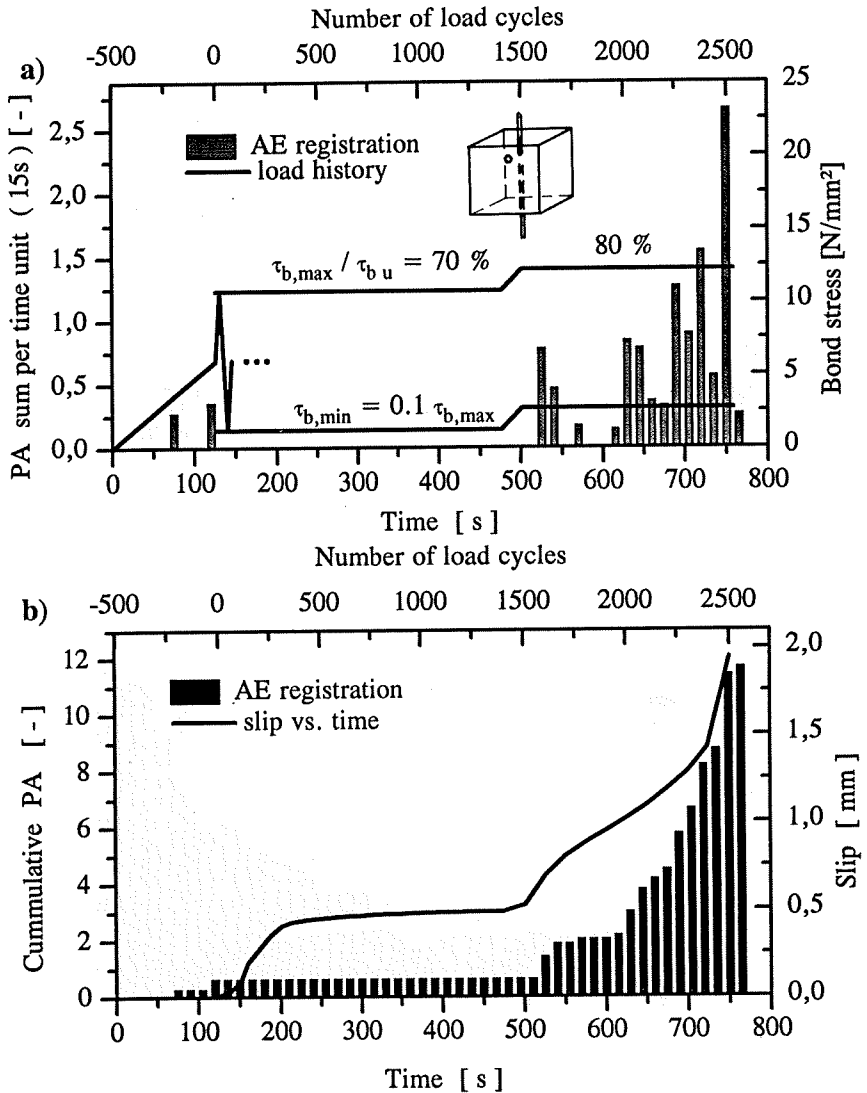
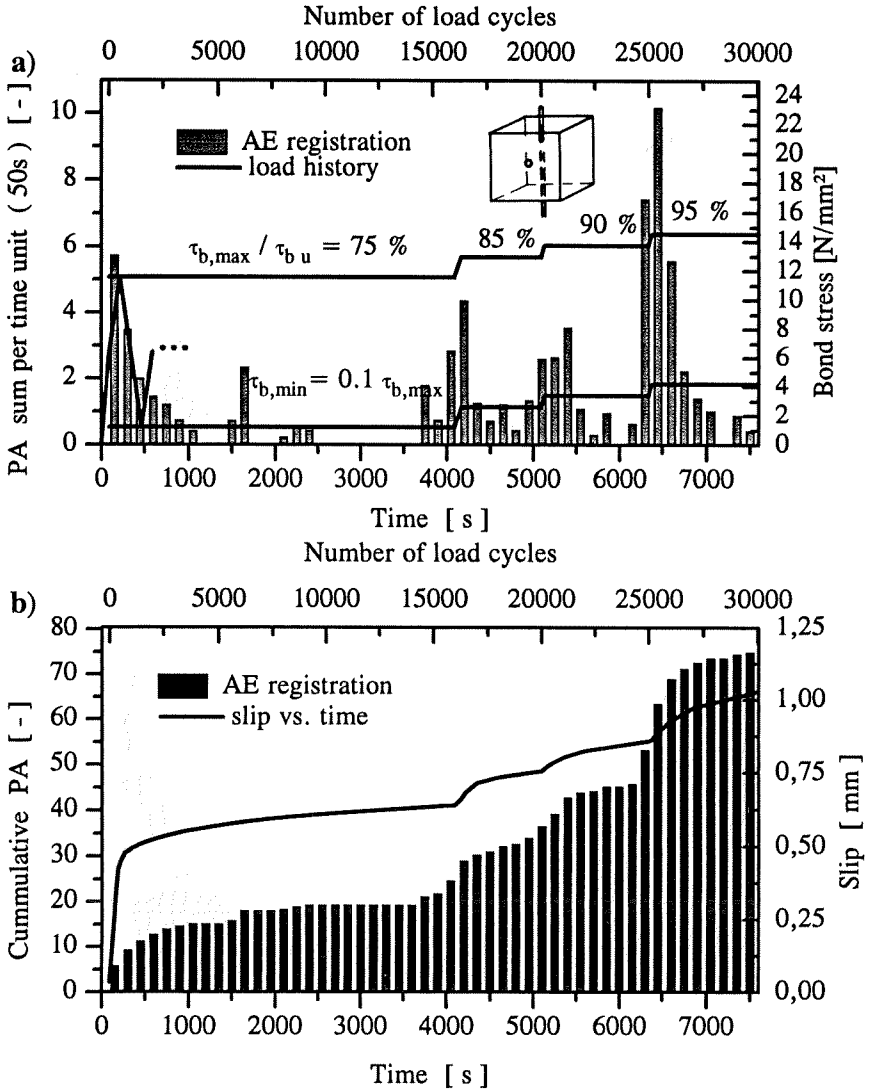


Fig.5 Cyclic pull-out test detecting acoustic emission signals ( $\varnothing 16$ ,  $\alpha_{sb} = 0.065$ ,  $f_y = 500 \text{ N/mm}^2$ ,  $l_b = 20 \text{ mm}$ ,  $f_c = 35 \text{ N/mm}^2$ )  
 a) PA sums in 10 sec intervals and  $\tau_b$  vs. time      b) Cum. PA vs. time



**Fig.6** Cyclic pull-out test detecting acoustic emission signals ( $\varnothing 16$ ,  $\alpha_{sb}=0.065$ ,  $f_y=500$  N/mm<sup>2</sup>,  $l_b=20$  mm,  $f_c=35$  N/mm<sup>2</sup>)  
**a)** PA sums in 15 sec intervals and  $\tau_b$  vs. time      **b)** Cum. PA vs. time



**Fig.7** Cyclic pull-out test detecting acoustic emission signals ( $\varnothing 16$ ,  $\alpha_{sb}=0.065$ ,  $f_y=500$  N/mm<sup>2</sup>,  $l_b=20$  mm,  $f_c=35$  N/mm<sup>2</sup>)

**a)** PA sums in 150 sec intervals and  $\tau_b$  vs. time    **b)** Cum. PA vs. time

### 4.3 Long term tests

Fig.8 indicates a relatively short (1200 s long) test result with a quasi-constant load and Fig.9 indicate a test result where the load was only once slightly increased in more than 3 days and then loaded up to failure. Non of them reached pull-out failure under the long term load.

Similarly to cyclic test results, acoustic emission signals were observed not only by reaching the load level but under the constant load as well (Figs.8.a and 9.a).

The accumulated damage also in this case shows a *correlation with the slip versus time relationship* (Figs.8.b and c).

## 5. CONCLUSIONS

From the analysis of *bond-slip behaviour* together with the *acoustic emission (AE) signals* registered in pull-out specimens having a very short bond length (two times rib spacing = 20 mm) subjected to monotonic, cyclic or long term loads, the following conclusions can be drawn:

- *Monotonic loading*: The slip and the AE registrations indicate similar tendencies, i.e., the highest AE amplitudes within a short time interval were registered also in the region of the highest bond stresses. The damage accumulation, defined as the cumulated AE amplitudes versus time diagram, has a point of inflexion at about reaching the bond strength.

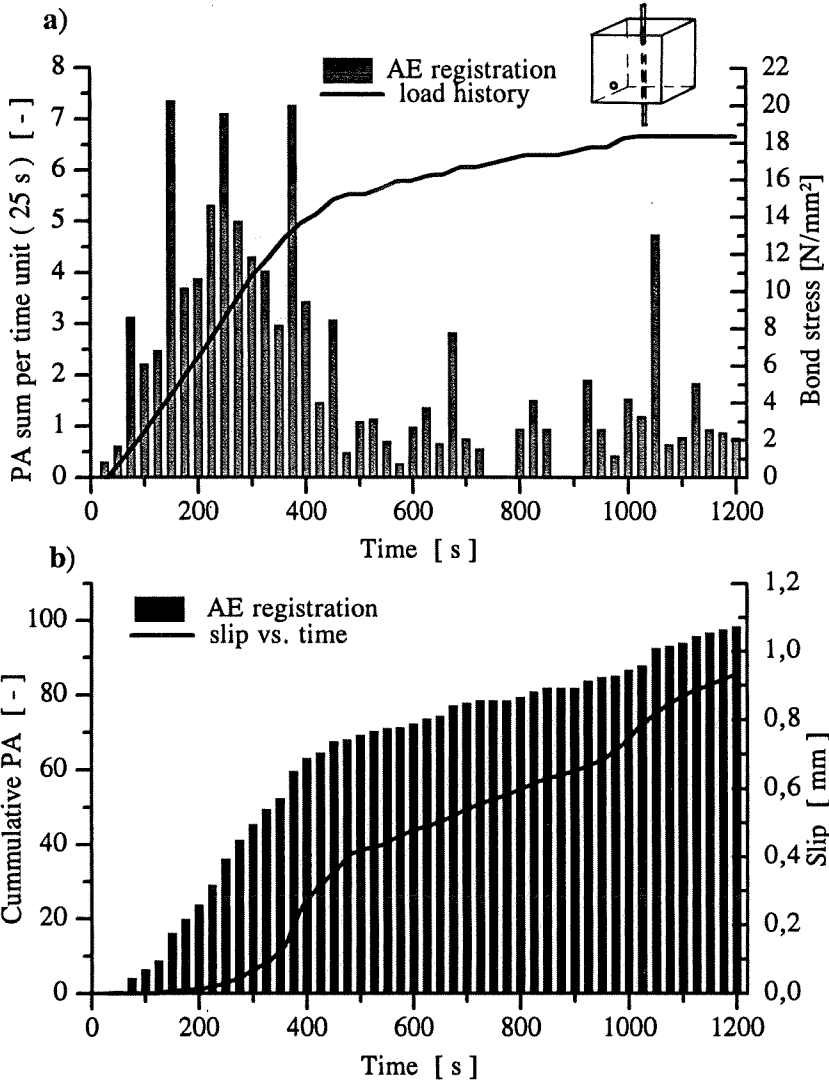


**Fig.8** Long term pull-out test detecting acoustic emission signals ( $\varnothing 16$ ,  $\alpha_{sb}=0.065$ ,  $f_y=500$  N/mm<sup>2</sup>,  $l_b=20$  mm,  $f_c=35$  N/mm<sup>2</sup>)  
**a)** PA sums in 25 sec intervals and  $\tau_b$  vs. time      **b)** Cum. PA vs. time

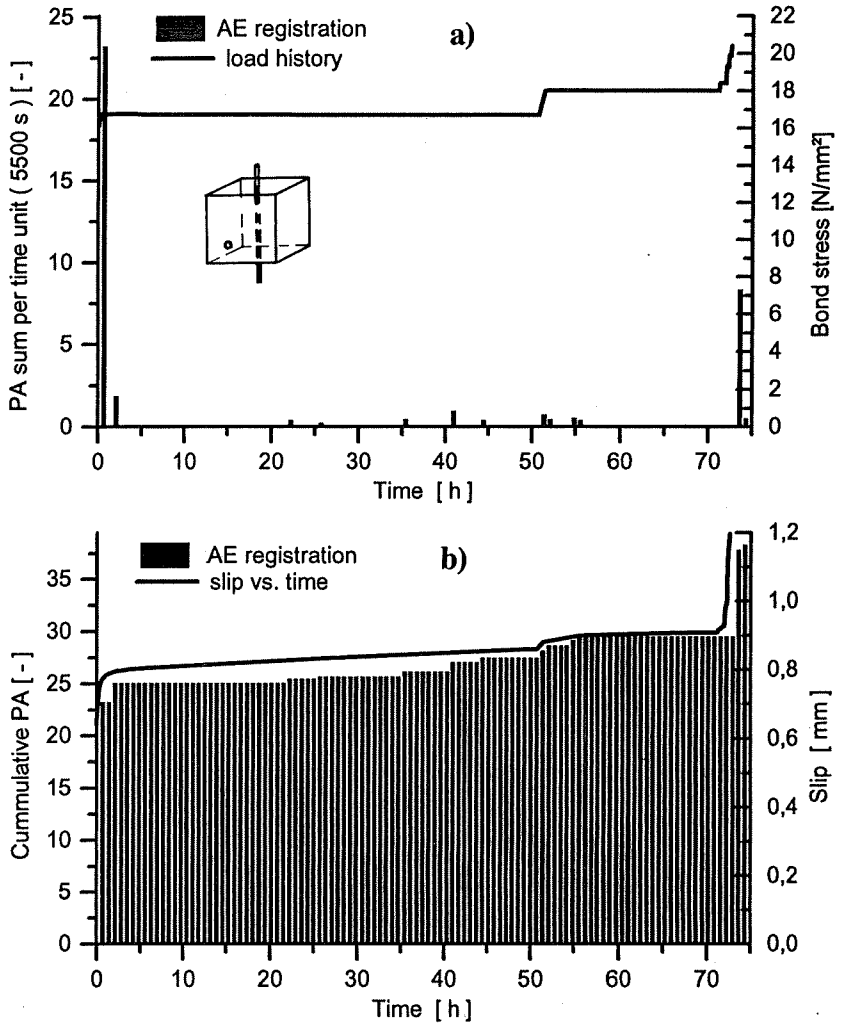


**Fig.9** Long term pull-out test detecting acoustic emission signals ( $\varnothing 16$ ,  $\alpha_{sb}=0.065$ ,  $f_y=500$  N/mm<sup>2</sup>,  $l_b=20$  mm,  $f_c=35$  N/mm<sup>2</sup>)  
**a)** AE amplitudes summed in 5500 sec intervals and bond stress vs. time  
**b)** Sum of AE amplitudes vs. time

- *Cyclic loading*: Most of the AE signals are registered at applying the initial monotonic load up to the mean value of the cyclic load, then at the beginning of the cyclic load and preceding the pull-out failure, however, signals were also detected during cycling with constant amplitude.
- *Long term loading*: similarly to cyclic tests, AE signals were observed not only by reaching the load level but under the constant load as well. The damage accumulation also indicates a similar tendency to the slip increase.
- The statistical analysis of the *AE signals* concerning time distribution and amplitude measurements is more accurate using the complete time signals of at least one sensor. With the time signal it is easy to distinguish between noise and AE signals.
- A set of at least four sensors (configured as an array of transducers) can be used for the *localization* of the events. This provides a basis for a comprehensive signal analysis concerning the fracture process.
- The *coherence function* was found to be a useful mathematical tool to compare signals with respect to the different fracture mechanisms demonstrated by them.

## 6. ACKNOWLEDGEMENTS

The authors are grateful to Wolfgang Staudenmeier and Wolfgang Albert for the operation with the hydraulic machine, to Till Cramer, Stefan Schempp, Bernd Weiler and Jens Kalsow for their help by the AE recording, to Markus Kinzle for the help in evaluation of measurements and last but not least to the German Research Society (**Deutscher Forschungsgemeinschaft**) for the financial support.

## 7. NOTATIONS

$\nu, k$	frequency value of a discrete fourier transform	Hz
$C_{xy}(\nu_1, \nu_2)$	coherence sum for two time series in a frequency range	-
$f_c$	mean value of concrete strength at testing measured on cubes of 150 side lengths	N/mm <sup>2</sup>
$f_y$	characteristic value of yield strength of reinforcing bar	N/mm <sup>2</sup>
$s$	relative displacement	mm
$t$	duration of load	s
$t^*$	time step of a discrete fourier transform	s
$\alpha_{sb}$	related rib area	-
$\tau_b$	bond stress	N/mm <sup>2</sup>
$\tau_{bu}$	bond strength obtained by monotonic load	N/mm <sup>2</sup>
$\tau_{b,max}$	maximum value of cyclic load	N/mm <sup>2</sup>
$\tau_{b,min}$	minimum value of cyclic load	N/mm <sup>2</sup>
$\tau_b/\tau_{bu}$	load level at long term load	%
$\tau_{b,max}/\tau_{bu}$	load level at cyclic load	%
$\emptyset$	nominal diameter of reinforcing bar	mm
PA	relative peak-to-peak amplitude	-

## 8. REFERENCES

- [1] Broms, B.B., "Technique for Investigation of Internal Cracks in Reinforced Concrete Members", ACI Journal, Vol.62, N°1, Jan. 1965, pp.35-43.

- [2] Goto, Y., "Cracks Formed in Concrete Around Deformed Tension Bars", *ACI Journal*, Vol.62, №1, January 1965, pp.71-93.
- [3] Goto, Y., Otsuka, K., "Studies on Internal Cracks Formed in Concrete Around Deformed Tension Bars", *ACI Journal*, Vol.68. №4, April 1971, pp.244-251.
- [4] Gambarova, P. and Giuriani, E., "Fracture Mechanics of Bond in Reinforced Concrete", *Discussion, Journal of Structural Engineering ASCE*, Vol.111. №5, May 1985, pp.1161-1164.
- [5] Rehm, G., "Über die Grundlagen des Verbundes zwischen Stahl und Beton", *Deutscher Ausschuß für Stahlbeton*, 1961, Heft 138
- [6] CEB, "Bond Action and Bond Behaviour of Reinforcement", *CEB Bulletin d'Information* №151, 1981
- [7] Martin, H., "Bond performace of ribbed bars (pull-out-ests): Influence of concrete composition and consistency", *Bond in Concrete, Proceedings*, Applied Science Publishers London, 1982, pp.289-299.
- [8] Soretz, S., Holzenbein, H., "Influence of Rib Dimensions of Reinfocing Bars on Bond and Bendability", *ACI Journal*, Vol.76, №1, January, 1979 pp.111-128.
- [9] Nagatomo, K., Kaku, T., "Bond behaviour of deformed bars under lateral compressive and tensile stress", *Proceedings of the Bond in Concrete Conference Riga, 1992*, pp.1-69 to 1-78
- [10] Vos, E., Reinhardt, H.W., "Bond stress-slip behaviour of deformed bars, plain bars and strands under impact loading", *Bond in Concrete, Proceedings*, Applied Science Publishers London, 1982, pp.173-182.
- [11] Rehm, G., Eligehausen, R., "Bond of Ribbed Bars Under High-Cycle Repeated Loads"; *ACI Journal*, Vol.76, №2, Feb. 1979, pp.297-309.

- [12] Eligehausen, R., Popov, E.P., Bertero, V.V., "Local Bond Stress-Slip Relationships of Deformed Bars Under Generalized Excitations", *Report* № UCB/EERC 82-23, Earthquake Engineering Research Center, University of California, Berkeley, California, Oct. 1983, 169 p.
- [13] Balázs G.L., "Fatigue of Bond", *ACI Materials Journal*, Vol.88, №6, Nov-Dec. 1991, pp.620-629.
- [14] Franke, L., "Einfluss der Belastungsdauer auf das Verbundverhalten von Stahl in Beton (Verbundkriechen)", *Deutscher Ausschuß für Stahlbeton*, 1976 Heft 268
- [15] Rostásy, F.S., Kepp, B., "Time-dependence of bond", *Bond in Concrete, Proceedings*, Applied Science Publishers London 1982, pp.183-192.
- [16] Palmgren, A., "Die Lebensdauer von Kugellagern", *Zeitschrift des Vereines deutscher Ingenieure*, April 1924, pp.339-341.
- [17] Oh, B.H., "Cumulative Damage Theory of Concrete under Variable Fatigue Loadings", *ACI Materials Journal*, Jan-Feb. 1991, pp.41-48.
- [18] Miner, M.A., "Cumulative Damage in Fatigue", *Journal of the Applied Mechanics*, Sept. 1945, pp.159-164.
- [19] Miller, R.K., McIntire, P. (ed.), "Nondestructive testing handbook", Vol.5, *Acoustic emission testing*, 2. ed., ASNT, 1987, 601 p.
- [20] Große, C., "Detection of cracks in reinforced concrete - an introduction to the problem with some measurements", *Otto-Graf-Journal*, Vol.2, 1991, pp.72-90.
- [21] Ohtsu, M., Shigeishi, M., Iwase, H., Koyanagi, W., "Determination of crack location, type and orientation in concrete structures by acoustic emission", *Mag. of concrete res.*, Vol.43, №1 155, 1991, pp.127-134.

- [22] Berthelot, J.M., Robert, J.L., "Modeling concrete damage by acoustic emission", J. of acoustic emission, Vol.6, №1, 1987, pp.43-60
- [23] Moczko, A., Stroeven, P., "Particle-matrix and steel fibre-matrix debonding reflected by acoustic emission recordings", *Proceedings*, "Bond in concrete" Conference, Riga, 1992, pp.1-120 to 1-129.
- [24] Stearns, D.S., "Digitale Verarbeitung analoger Signale", *Verlag Oldenburg*, 2. Ed. 1984.
- [25] Digital signal processing committee of the IEEE (ed.), "Programs for digital signal processing", *IEEE Press*, Wiley & sons, New York, 1979.
- [26] Hesselmann, N., "Digitale Signalverarbeitung", *Vogel-Buchverlag*, Würzburg, 1983.